Catalytic effects of magnetic and conductive nanoparticles on immobilized glucose oxidase in skin sensors.

To cite this article before publication: Lilian C. Alarcon Segovia *et al* 2021 *Nanotechnology* in press https://doi.org/10.1088/1361-6528/ac0668

Title: Catalytic effects of magnetic and conductive nanoparticles on immobilized glucose oxidase in skin sensors.

Authors: Lilian C. Alarcón-Segovia,[a,b] Amay J. Bandodkar,[c] John A. Rogers[c] and Ignacio Rintoul.[a]

[a] Instituto de Desarrollo Tecnológico para la Industria Química. Universidad Nacional del Litoral and Consejo Nacional de Investigaciones Científicas y Técnicas. Santa Fe, Argentina.

[b] Universidad María Auxiliadora, Asunción, Paraguay.

[c] Querey Simpson Institute for Bioelectronics. Northwestern University. Evanston, USA.

Abstract: Wearable skin sensors is a promising technology for real-time health care monitoring. They are of particular interest for monitoring glucose in diabetic patients. The concentration of glucose in sweat can be more than two orders of magnitude lower than in blood. In consequence, the scientific and technological efforts are focused in developing new concepts to enhance the sensitivity, decrease the limit of detection (LOD) and reduce the response time (RT) of glucose skin sensors. This work explores the effect of adsorbed superparamagnetic (MNPs) and conductive nanoparticles (CNPs) on carbon nanotube substrates (CNTs) used to immobilize glucose oxidase enzyme in the working electrode of skin sensors. MNPs and CNPs are made of magnetite and gold, respectively. The performance of the sensors was tested in standard buffer solution, artificial sweat, fresh sweat and on the skin of a healthy volunteer during an exercise session. In the case of artificial sweat, the presence of MNPs accelerated the RT from 7 s to 5 s at the expense of increasing the LOD from 0.017mM to 0.022 mM with slight increase of the sensitivity from 4.90 $\mu AmM^{-1}cm^{-2}$ to 5.09 $\mu AmM^{-1}cm^{-2}$. The presence of CNPs greatly accelerated the RT from 7 s to 2 s and lowered the LOD from 0.017 mM to 0.014 mM at the expense of a great diminution of the sensitivity from 4.90 $\mu AmM^{-1}cm^{-2}$ to 4.09 $\mu AmM^{-1}cm^{-2}$. These effects were explained mechanistically by analyzing the changes in the concentration of free oxygen and electrons promoted by MNPs and CNPs in the CNTs and its consequences on the the glucose oxidation process.

Keywords: nanomagnetite; nanogold; integrated electronics; biomaterials; biosensors; diagnostics;

diabetics

1 Introduction

Diabetes mellitus is defined as a chronic metabolic disorder of the glucose level in blood. Glucose is the main fuel of the body. Glucose enters the cells from the blood stream with the help of the insulin hormone. Diabetes is caused by an alteration in the metabolism of insulin and/or due to the damage of insulin producer β pancreatic cells. According to the World Health Organization, diabetes is the eighth leading cause of death with 2.2% of total deaths Worldwide [1–5]. The International Diabetes Federation forecast 693 million people will suffer from diabetes by 2045 [6].

The diagnosis and control of diabetes require strict monitoring of blood glucose levels [7–9]. People that self-monitor their glucose levels can easily take control of the disease. Digital finger-sticks are the best known medical devices used for point of care monitor blood glucose levels. These devices are based on taking blood samples by self-inflicted punctures in the fingers. Therefore, they are considered as invasive, painful, uncomfortable, promoters of psychological stress and with risk of infection [10–12].

The current technological challenge is to provide non-invasive, lightweight, flexible and ultra-fine devices to measure glucose levels from the comfort of the patient [13-16]. Recently, minimally invasive devices have been developed. These sensors are designed to monitor glucose levels in blood indirectly by measuring the glucose level in other body fluids such as sweat, tears or saliva [11,17,18]. The correlations between the glucose concentration in sweat and blood is well know and can be found in the literature [19,20].

Sweat is a complex solution secreted by sweat glands. Sweat solution is clear, odorless and composed mostly of water and sodium chloride (NaCl). It also contains other metabolites such as potassium, calcium, magnesium, amino acids, urea, lactate, lactic acid, ascorbic acid, uric acid and glucose [21]. Glucose levels in healthy and diabetic persons range from 0.06 mM to 0.11 mM and from 0.01 mM to 1 mM, respectively [20]. It is important to mention that the pH of sweat may vary from 4 to 7 [22–25].

Several technologies are been used to develop medical devices based on skin sensors. These sensors work in direct contact with the skin, have the ability to adapt to the irregular surfaces and support the tensions generated by body motion [26–31]. The sensors are capable of measuring tiny currents generated by the selective oxidation of glucose using glucose oxidase enzyme (GOx). The need for improving the sensor's sensitivity, limit of detection (LOD) and response time (RT) has

pushed the scientific interest to explore nanomaterials with catalytic properties over the GOx activity. Magnetite nanoparticles (MNPs) and gold nanoparticles (CNPs) have been tried as catalysts to enhance the GOx activity during the oxidation of glucose in blood samples [32–35]. Moreover, magnetic fields can accelerate organic reactions by interacting with unpaired electrons [36-38]. Carbon nanotubes (CNTs) were successfully used to bind GOx to the electrode substrates of several glucose skin sensors [20,39–42]. Yet, the potential use of MNPs and CNPs to improve the performance of GOx immobilized in CNTs deserves further investigation [43].

In this contribution we propose to evaluate the effects of MNPs and CNPs on sensors intended for the detection of glucose in sweat. The performance of the sensors were evaluated experimentally in standard buffer solution, artificial sweat, human fresh sweat and on the skin of a healthy volunteer during an exercise session. Their effects on the sensitivity, LOD, RT, glucose selectivity in presence of other metabolites and response at different physiologically relevant pH values were studied. Finally, a mechanistic explanation of the effects of MNPs and CNPs on the performance of catalytic properties of immobilized GOx in different media is presented.

2 Experimental Part

2.1. Materials.

Ultra-pure ferric chloride hexahydrate, $FeCl_3 \cdot 6H_2O$, (Biopack, Argentina), ultra-pure ferrous chloride tetrahydrate, $FeCl_2 \cdot 4H_2O$, (Biopack, Argentina), ammonium hydroxide aqueous solution, NH_4OH, 28% w/w (Anedra, Argentina), ultrapure N_2 gas grade 4.5 (Indura, Argentina), tetrachloroauric acid (Sigma Aldrich, USA), trisodium citrate (Sigma Aldrich, USA), H_2O of Millipore quality with resistivity of 18.2 MΩ and density $\delta w = 0{,}99704$ g cm^{-3} and absolute methanol (Cicarelli, Argentina) were used as iron sources, pH regulator, non-oxidant atmosphere, gold source, reducing agent, reaction medium and swashing solvent, respectively. The reactants were used for the synthesis of MNPs and CNPs.

CNTs paper of ø = 2 mm (Bucky paper, GSM 20; Nanotech Labs, USA), polyamide (Argon Inc., USA), conductive silver/silver chloride ink (E2414, Ercon Inc., USA), silver epoxy (Epoxi 8331, MG Chemicals, USA), glucose oxidase (GOx) from Aspergillus niger, Type X-S (EC 1.1.3.4) (Sigma, USA) and chitosan (Aldrich, USA) were used to fabricate the sensors.

Bovine serum albumin (Sigma Aldrich, USA), tetrathiafulvalene (Sigma Aldrich, USA), D-(+)-glucose (Sigma, USA), artificial human perspiration (Pickering, USA), phosphate buffer pH = 7.0 (Sigma Aldrich, USA), acetic acid (Fisher Scientific, USA), uric acid, L-(+)- ascorbic acid (Sigma, USA), L-(+)-lactic acid (Sigma, USA) were used to prepare the testing media.

Natural fresh human perspiration was collected from the arm of a healthy volunteer. To induce perspiration, the volunteer underwent a pedaling exercise session on a stationary bicycle. Previously, the volunteer's arm was shaved and sanitized to avoid any contamination.

2.2. Synthesis of MNPs.

MNPs were synthesized using a co-precipitation method [44]. First, an aqueous solution of $FeCl_3 \cdot 6H_2O$ and $FeCl_2 \cdot 4H_2O$ was prepared. The molar ratio between $FeCl_3$ / $FeCl_2$ = 2. Second, the solution was put under stirring at moderated speed and thermostatted at 50 ºC. Third, 30 ml of NH_4OH 28% w/w solution per each 0.07 mol of iron were added to induce the precipitation of Fe_3O_4 MNPs. The precipitation reaction was left to proceed during 60 minutes under N_2 atmosphere. The stirring speed and temperature were kept constant during all the experiment. Fourth, the obtained dark precipitate was washed with deionized water to remove Cl^- ions and the remaining NH_4OH. The decantation of the precipitate was assisted using strong neodymium magnets. Subsequently, the precipitate was washed with methanol and magnetically decantated again. And finally, it was vacuum dried for approximately 45 minutes and then stored in a hermetically sealed container.

2.3. Synthesis CNPs.

CNPs have been obtained by a modified Turkevich method [45,46]. The procedure began with the preparation of an aqueous solution of 1 millimolar of tetrachloroauric acid and another aqueous solution of 38.8 millimolar of trisodium citrate dihydrate. The tetrachloroauric acid solution was heated under moderate agitation to the boiling point. Subsequently, the dehydrated trisodium citrate solution was added drop by drop and the agitation was slightly increased. The reaction was left to proceed during 15 minutes. The color of the resulting solution switched from light yellow to wine red indicating the formation of gold CNPs. The synthesis product was allowed to cool to room temperature, filtered with a 0.22 µm membrane and stored in a glass flask until use.

2.4. Nanomaterials characterization.

The purity, the degree of crystallinity and the size of the ordered domains of the MNPs and CNPs were measured using a X-ray diffractometer (X-ray Diffractometer Model XD-D1 Shimadzu, Japan) operating with a Cu-Kα X-ray source with wavelength λ = 1.54 Å. The size of the particles were measured using a high-resolution transmission electron microscope (JEOL 100 CX II) operating at 100 kV and magnifications of 270000x – 450000x. The software of the microscope permitted to discriminate, count, measure and perform statistical analysis of the particles. The magnetization and

magnetic saturation of the MNPs were characterized using a Vibrating Sample Magnetometer (VSM). The reflection spectra of the CNPs were measured using a UV-Vis spectrometer (Lambda1050 Perkin, USA).

2.5. Preparation of solutions.

A 0.1 M tetrathiafulvalene solution was prepared by dissolving tetrathiafulvalene in an acetone/ethanol (1:9 v/v) solution. A GOx solution was prepared by dissolving 40 mg/ml of GOx in 0.1 M of phosphate buffer containing 10 mg/ml of bovine serum albumin. A chitosan solution was prepared by dissolving 1% of chitosan in 0.1 M acetic acid aqueous solution. A MNPs suspension was prepared by dispersing 1 mg/ml of MNPs in 0.1 M phosphate buffer. The CNPs suspension was directly taken from the reaction medium obtained in section 2.3.

2.6. Fabrication of electrode substrates.

The sensors were composed of three parts: a reference electrode (RE), a working electrode (WE) and a contact electrode (CE). The basic structure of each electrode was formed by deposition of a 10 nm chromium layer on a 75 μm polyamide film. Then, a 100 nm gold layer was deposited over the chromium layer. The polyamide film brings structure and mechanical resiliency of the electrode, the chromium layer is an adhesion layer and the gold layer is current collector. The deposition of chromium and gold were carried out by means of an electron bean evaporation (AJA International Inc., USA). Finally, the electrodes were cut using a UV laser (LPKF, Germany).

2.7. Preparation of glucose sensors.

The contact pad of the electrodes were bonded to conductive wires using silver epoxy cured at 143 °C for 15 minutes. Subsequently, CNTs papers were bonded to the gold layer of the WEs using a carbon conductive ink and baking them at 100 ºC for 10 min. Then, the drop casting technique was employed to functionalize the WEs of the sensors. Three different functionalization routes were applied to obtain three classes of sensors: Type 1, Type 2 and Type 3.

Type 1 sensors were obtained by drop casting the exposed surface of the CNTs paper with 2μL of the tetrathiafulvalene solution, 4 μL of the GOx solution and 2μL of the chitosan solution. Type 2 sensors were obtained by drop casting the exposed surface of the CNTs paper with 2μL of the tetrathiafulvalene solution, 8 μL of a suspension of 1 mg of MNPs per 1ml of the GOx solution and 2μL of the chitosan solution. And, Type 3 sensors were obtained by drop casting the exposed surface of the CNTs paper with 2μL of the tetrathiafulvalene solution, 14 μL of a suspension composed

of 10 μL CNPs and 4 μL of GOx solution and 2μL of chitosan solution. Finally, Type 1, Type 2 and Type 3 sensors were kept at 4 °C until use.

2.8. Electrochemical characterization of glucose sensors.

The characterizations were performed at 37 ºC using a potentiostat (Metrohm Autolab, model PGSTAT 128N, The Netherlands). The responses of Type 1, Type 2 and Type 3 sensors were evaluated at different glucose concentrations in standard buffer solution and artificial sweat. The glucose concentrations in standard buffer solution and artificial sweat were 0 mM, 0.25 mM, 0.50 mM, 0.75 mM and 1.00 mM. Such range of glucose concentration corresponds to human sweat [20]. Three samples per experiment were tested and each measurement was replicated three times to confirm the reproducibility of results.

The RT was measured as the time required to reach the 95% of the sensor steady state response. The LOD was measured, according to IUPAC, as the lowest quantity of a substance that can be distinguished from the absence of that substance with a stated confidence level of 99%. The lineal range was defined as the substance concentration range in which the sensor response changes linearly. In this contribution, $R^2 > 0.995$ was considered as linear.

The steady state current responses of the sensors obtained in different media were plot against their corresponding glucose concentrations. The sensitivity values of the sensors were calculated as the slope of the obtained plots divided the area of the electrodes. The area of the electrodes was calculated as: πr^2. The radius of the electrodes were 1 mm. Minimal steady state currents needed to produce a signal 100 times higher than the electrical noise basal current to be considered as significant.

The glucose selectivity of the sensors in artificial sweat at 37 ºC with added interfering metabolites was also tested. It is known that lactic acid, ascorbic acid and uric acid can greatly interfere the response of glucose sensors [47]. The glucose selectivity of the sensors was tested in media designed with increasing levels of interference power: artificial sweat; artificial sweat + 1 mM of glucose; artificial sweat + 1 mM of glucose + 1 mM of lactic acid; artificial sweat + 1 mM of glucose + 1 mM of lactic acid + 1 mM of ascorbic acid; artificial sweat + 1 mM of glucose + 1 mM of lactic acid + 1 mM of ascorbic acid + 1 mM of uric acid and artificial sweat + 2 mM of glucose + 1 mM of lactic acid + 1 mM of ascorbic acid + 1 mM of uric acid. These concentrations of interfering metabolites correspond to their usual physiological levels in natural sweat [48].

It is also known that the response of glucose sensors can be greatly affected by the pH variations of the human sweat. Therefore, the response of the sensors to glucose concentrations in the range between 0 mM to 1 mM in artificial sweat at 37 ºC was tested at three physiologically relevant pHs:

4.5, 5.5 and 6.5.

Subsequently, the sensors with the best performance against interfering metabolites and pH variation were tested in human fresh sweat at pH = 5 and 37 ºC. The fresh sweat was collected from the skin of a healthy, non-diabetic, 32 years old, male volunteer. The volunteer performed physical exercise by pedaling a stationary bicycle set in moderate resistance during 20 minutes. The fresh sweat was collected using a spatula. The sensitivity, LOD and RT were measured and compared with those obtained in buffer solution and artificial sweat. Finally, these sensors were integrated and tested on the skin of the same healthy volunteer. The sensors were placed on the epidermis of the forearm of the volunteer. The volunteer performed physical exercise by pedaling a stationary bicycle set in moderate resistance during 20 minutes. The data acquisition was started when sweat began to segregate in the epidermis of the volunteer. The profuse segregation of sweat started approximately after 3 minutes of pedaling. The current signal associated to the glucose level measured by the sensor in the volunteer was compared against the qualitative result of a standard colorimetric assay [40].

3 Results and discussion

3.1. Characterization of MNPs.

Figures 1(a), 1(b) and 1(c) show a TEM image, the XRD, and the VMS analysis of MNPs, respectively. The XDR pattern of peak positions and intensities is very well correlated with the values for magnetite reported in the literature. No odd peaks were identified in the diffractometer. The absence of odd peaks is an evidence of the absence of any compound different than magnetite [49]. This result indicates that the obtained precipitate is composed of pure magnetite. The average crystallite size of MNPs was calculated using a Debye-Scherrer equation based routine available in the software of the XRD device. The average crystallite size resulted 8.7 nm. The TEM image shows near spherical shape of the MNPs. The average particle size of MNPs was calculated using a routine based on statistical image analysis available in the software of the TEM device. The average particle size resulted 9.0 nm. The fact that the cristallite size is 97% of the particle size indicates that the MNPs are almost 100% monocristalline. VSM analysis shows the absence of hysteresis loops and the levels of magnetic saturation. The results are clear indicators of the superparamagnetic behavior of the MNPs [50]. Conclusively, the synthesis protocol resulted in pure monocrystalline superparamagnetic spherical magnetite nanoparticles.

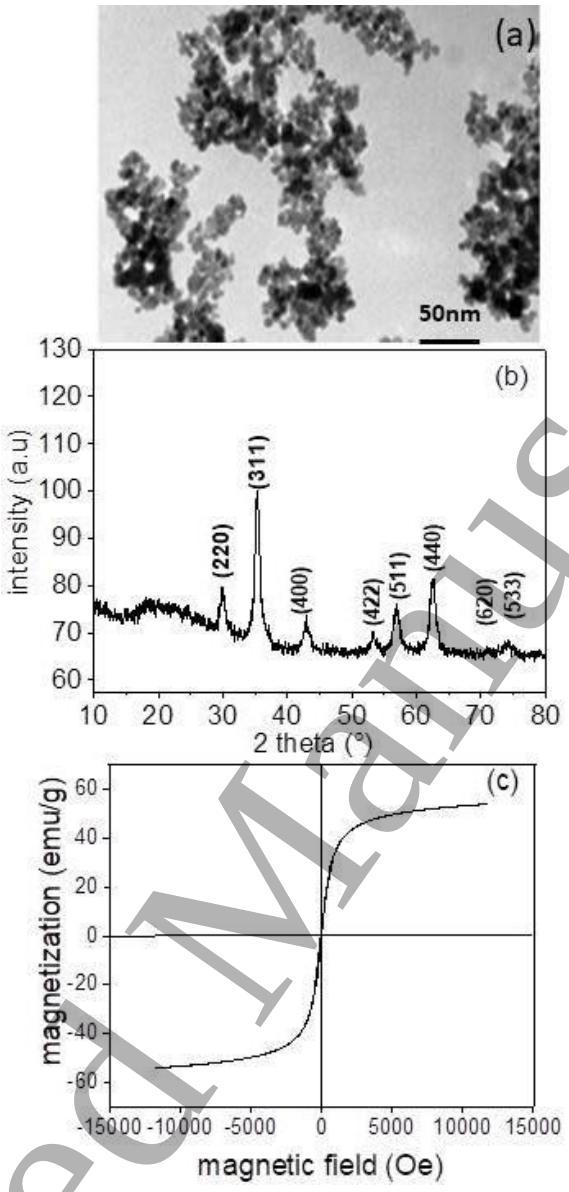

Figure 1. Characterization of MNPs: (a) TEM image; (b) X-ray diffraction pattern; and (c) Magnetization curve.

3.2. Characterization of CNPs.

Figures 2(a), (b) and (c) show a TEM image, the XRD, and the absorption spectra of the CNPs. The XDR pattern of peak positions and intensities is very well correlated with the values for gold reported in the literature [51]. The absence of odd peaks is an evidence of the absence of any compound different than gold. This result indicates that the obtained precipitate is composed of pure gold. The absorption spectra shows an absorption band around 525 nm which is an standard indicator of the formation of pure gold nanoparticles [33,52]. Gold is an excellent conductor of electricity. The TEM image shows near spherical shape of the CNPs. It also shows some degree of aggregation. The average

particle size of CNPs was calculated using a routine based on statistical image analysis available in the software of the TEM device. The average particle size resulted 12.6 nm.

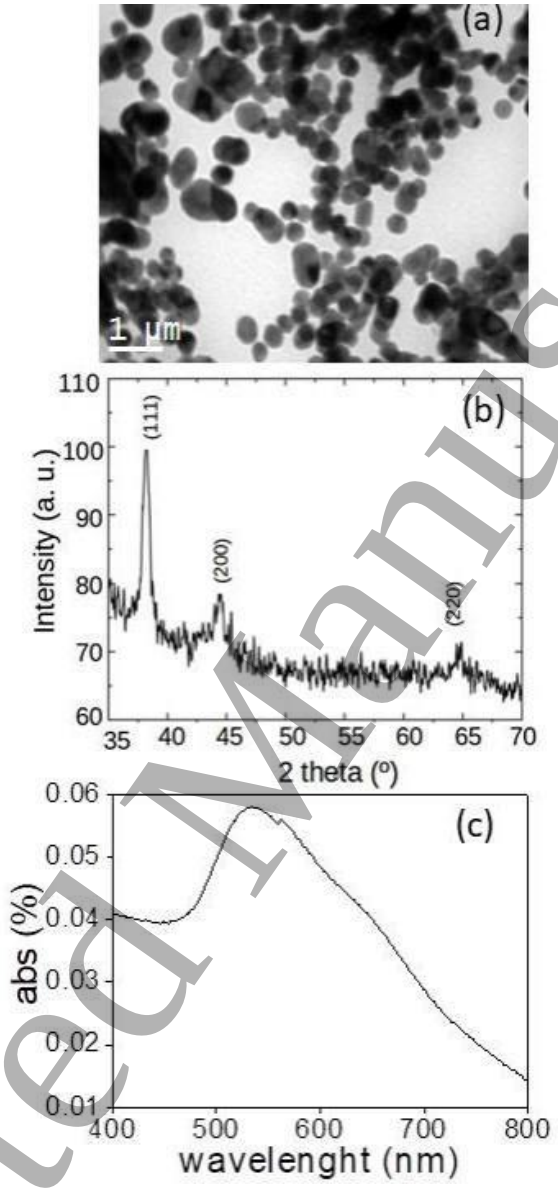

Figure 2. Characterization of CNPs: (a) TEM image; (b) X-ray diffraction pattern; and (c) Absorption spectra.

3.3. In-vitro electrochemical characterization of sensors.

Figure 3 shows exemplary the chrono-amperometric response of a Type 1 sensor to the presence of glucose at different concentrations in artificial sweat. The RT, LOD and sensitivity of the sensors were measured according to Section 2.8.

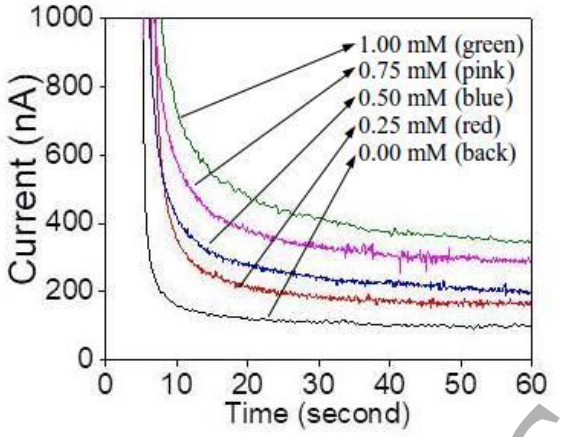

Figure 3. Chrono-amperometric responses of a Type 1 sensor in artificial sweat at pH = 5.0 and T = 37ºC. Glucose concentrations: 0.00 mM (back); 0.25 mM (red); 0.50 mM (blue); 0.75 mM (pink) and 1.00 mM (green). Potential step: 0.01 V (vs Ag/AgCl).

Table 1 summarizes the resulting parameters of Type 1, Type 2 and Type 3 sensors in the presence of glucose at different concentrations in standard buffer solution and artificial sweat.

Type 1 and Type 2 sensors presented a sensitivity almost two times higher than Type 3 sensors when tested in buffer solution. Interestingly, Type 1 and Type 2 sensors presented nearly 25% higher sensitivity than Type 3 sensors when tested in artificial sweat. Type 2 and Type 3 sensors presented almost half the RT (~5 seconds) than Type 1 sensors (~9 seconds) when tested in buffer solution. However, Type 3 sensors resulted with significantly lower RT (~2 seconds) than Type 1 (~7 seconds) and Type 2 (~5 seconds) sensors when tested in artificial sweat. Type 3 sensors presented the lowest LOD followed by Type 1 and Type 2 sensors in both, buffer solution and artificial sweat. Interestingly, LOD is slightly lower in buffer solution than in artificial sweat for all sensors.

Table 1. Performance of Type 1, Type 2 and Type 3 glucose sensors.

Sensor	**Testing medium**	**Sensitivity ($\mu AmM^{-1}cm^{-2}$)**	**LOD (mM)**	**RT (seconds)**
Type 1	Phosphate buffer	16.90	0.013	9
Type 2	Phosphate buffer	15.30	0.017	5
Type 3	Phosphate buffer	8.60	0.012	5

Type 1	Artificial sweat	4.90	0.017	7
Type 2	Artificial sweat	5.09	0.022	5
Type 3	Artificial sweat	4.09	0.014	2
Type 1	Fresh sweat	2.50	0.069	6

Common conditions and results: Temperature: 37 ºC. Range of glucose concentration: 0-1 mM. Confirmed linear range: 0-1 mM with $R^2 > 0.995$.

Figure 4 shows the effect of selected interfering species on the chrono-amperometric responses of Type 1 and Type 2 sensors in artificial sweat. Type 1 and Type 2 sensors were selected for the chemical interference study because they presented the highest sensitivity in artificial sweat.

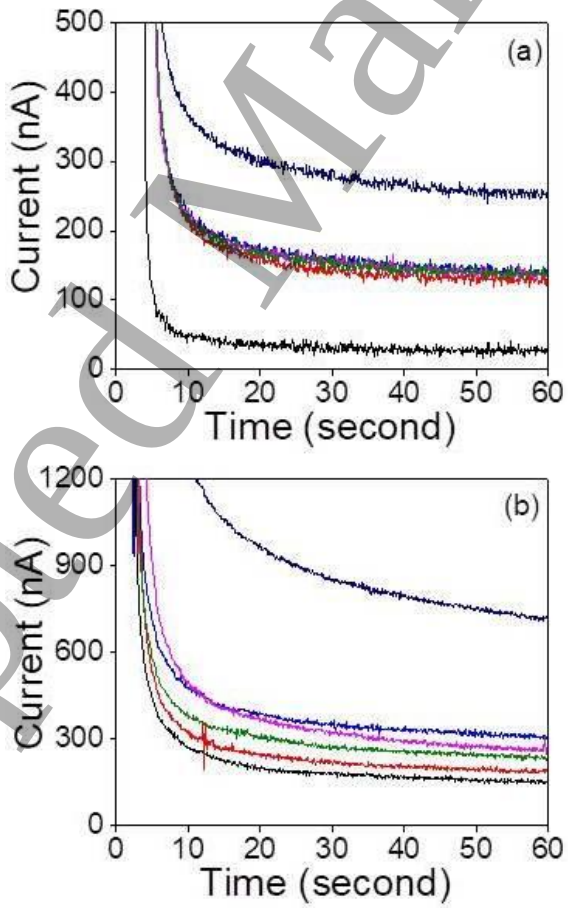

Figure 4. Interference studies: (a) Type 1 sensor; (b) Type 2 sensor. Black: artificial sweat. Red: artificial sweat + 1 mM of glucose. Green: artificial sweat + 1 mM of glucose + 1 mM of lactic acid.

Violet: artificial sweat + 1 mM of glucose + 1 mM of lactic acid + 1 mM of ascorbic acid. Blue: artificial sweat + 1 mM of glucose + 1 mM of lactic acid + 1 mM of ascorbic acid + 1 mM of uric acid. Dark blue: artificial sweat + 2 mM of glucose + 1 mM of lactic acid + 1 mM of ascorbic acid + 1 mM of uric acid. Temperature: 37 ºC. Potential step: 0.01 V (vs Ag/AgCl).

Clearly, Type 1 sensors resulted insensitive to the presence of interfering metabolites and their mixtures even at large quantities. Moreover, it is also evident the increment of the response signal when the glucose concentration increased from 0 mM to 1 mM and 2 mM.

Conversely, Type 2 sensors greatly varied their response signals according to different compositions of the interfering media. However, the sensors responded correctly with an evident increment of the signal current when the glucose concentration increased from 0 mM to 1 mM and 2 mM. Indeed, Type 2 sensors may be useful to develop monitoring dermal devices for medical conditions that manifest with abnormal levels of lactic, ascorbic and uric acids. Monitoring of stress, vitamin C level, control of gout disease and other metabolic disorders by measuring lactic, ascorbic and uric acids in sweat can be mentioned as examples [53].

Type 1 sensors were selected for the pH study because they resulted unaffected by interfering metabolites. Figure 5 shows the steady state current signals of a Type 1 sensor as function of glucose concentration in artificial sweat at different pHs. Clearly, Type 1 sensors keep their linear responses at pH = 4.5, 5.5 and 6.5. However, significant decrease in sensitivity is reported at pH = 4.5. This can be attributed to partial deactivation of the GOx enzyme at pH = 4.5.

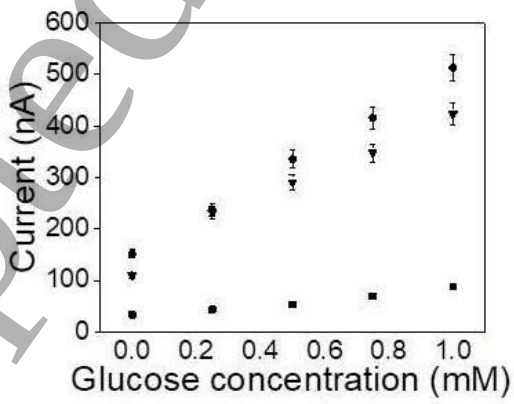

Figure 5. Steady state signal responses of a Type 1 sensor versus glucose concentration at different pHs in artificial sweat. T = 37 ºC. pH = 4.5 (■); pH = 5.5 (▼) and pH = 6.5 (●).

3.4. Ex-vivo electrochemical characterization of sensors.

Based on precedent results, Type 1 sensors were selected for tests in fresh sweat. Figure 6 shows

that the steady state current signal of a Type 1 sensor in fresh sweat increases linearly according to the increase of the glucose concentration from 0 mM to 1 mM. The sensitivity of Type 1 sensors in fresh sweat resulted 2.50 $\mu AmM^{-1}cm^{-2}$ with RT = 6 seconds and LOD = 0.069 mM. Table 1 may serve to compare the performance of Type 1 sensors in buffer solution, artificial sweat and fresh sweat. Clearly, the sensitivity of Type 1 sensors in fresh sweat is 49% and 85% lower than its sensitivity in artificial sweat and buffer solution, respectively. The LOD in fresh sweat resulted 4 and 5 times higher than in artificial sweat and buffer solution, respectively. And the RT resulted slightly lower in fresh sweat than in artificial sweat and still significantly lower than in buffer solution.

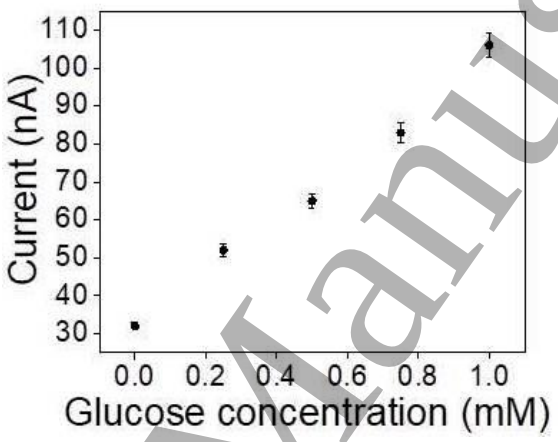

Figure 6. Steady state signal responses versus glucose concentration of a Type 1 sensor in fresh sweat at pH = 5 and T = 37 ºC.

3.5. *In-vivo electrochemical characterization of sensors.*

Type 1 sensor was tested on the skin of a volunteer during an exercise session. Figure 7 shows a Type 1 sensor installed on the volunteer's skin and the real-time monitoring of glucose in sweat during an exercise session. Clearly, a signal is obtained as soon as sweat started to exude from the skin of the volunteer. The signal slightly increased up to nearly 450 seconds. Then, a sharp increment of the signal was registered in the range between 450 to 700 seconds to finally reach a plateau until the end of the experiment. The intensity of the signal was well corresponded with qualitative standard colorimetric results.

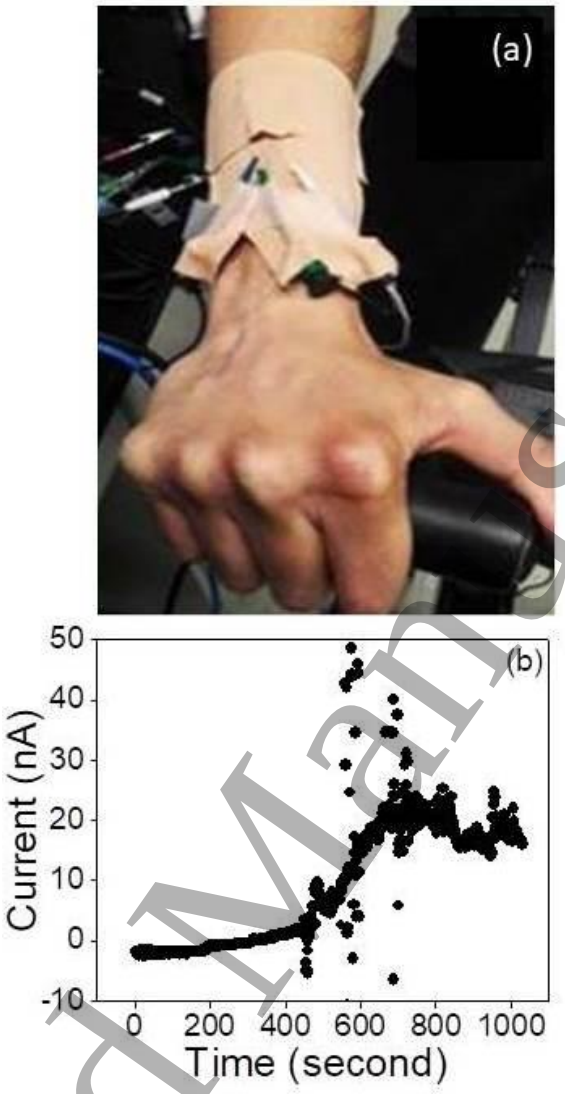

Figure 7. (a) Type 1 sensor installed on the volunteer's skin. (b) Chrono-amperometric real-time response to glucose in sweat.

3.6. Analysis of the effect of MNPs and CNPs on the performance of sensors.

The effect of MNPs can be appreciated by comparing the performances of Type 2 against Type 1 sensors in buffer solution and artificial sweat. In buffer solution, the presence of MNPs caused 9% diminution of the sensitivity, 31% increase of the LOD and 44% decrease of the RT. In artificial sweat, they caused 4% increment of the sensitivity, 29% increase of the LOD and 29% decrease of the RT. In general, it can be stated that the presence of MNPs accelerated the RT at the expense of increasing the LOD without clear changes in the sensitivity. Figure 8 proposes a mechanistic explanation of this behavior. The presence of MNPs provides a large surface where the equilibrium between magnetite and ferric and ferrous oxides may occurs with further generation of free oxygen [54]. The abundance of

oxygen in the substrate where the GOx enzyme reacts with glucose is proposed to accelerate the reaction which in turns is evidenced as an important decrease of the RT [55,56]. It is also evident that magnetite and the associated equilibrium between ferric oxide and ferrous oxide do not interfere with glucose and GOx activities justifying the slight changes in sensitivity. Finally, it is also evident that the presence of MNPs increases somehow the activation energy of glucose oxidation promoting the need of higher glucose concentration to activate the reaction and thus an increment of the LOD. It is hypothesized that the increase of the activation energy may be a consequence of the shortage of electrons in the GOx substrate due to the function of electron sink of the oxide lattice of the MNPs [55,56]. Those electrons will not be available for the glucose oxidation reaction increasing the potential required to overcome the activation energy.

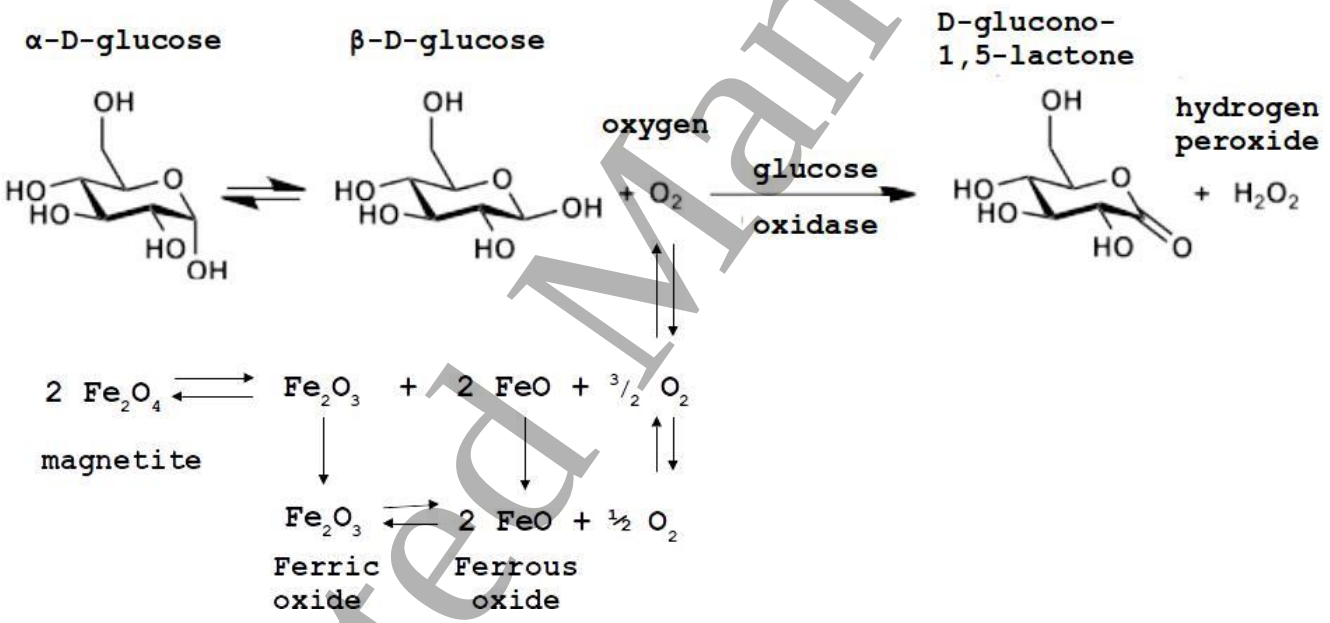

Figure 8. Proposed mechanism for MNPs effects on the GOx induced glucose oxidation process.

The effect of CNPs can be appreciated by comparing the performances of Type 3 against Type 1 sensors in buffer solution and artificial sweat. In buffer solution, the presence of CNPs caused 49% diminution of the sensitivity, 8% decrease of the LOD and 44% decrease of the RT. In artificial sweat, they caused 17% diminution of the sensitivity, 18% decrease of the LOD and 71% decrease of the RT. In general, it can be stated that the presence of CNPs greatly accelerated the RT and lowered the LOD at the expense of a great diminution of the sensitivity. The presence of CNPs provides an incredible large amount of labile electrons useful to facilitate electron transfer within reactive species. Gold has

the electronic structure: [Xe] $4f^{14}$ $5d^{10}$ $6s^1$. The very high mobility of the unpaired electron in the 6S orbital and the very high surface/volume ratio of gold nanoparticles promote the abundance of electrons in the substrate where the GOx enzyme reacts with glucose. This electronic abundance makes the glucose oxidation to proceed very fast which in turns is evidenced as an important decrease of the RT. The abundance of electrons also decreases the activation energy of glucose oxidation allowing to be detected at lower glucose concentration which in turns is evidenced as a decrease of the LOD. It is also evident that the electrons interfere with glucose and GOx activities justifying the decrease of sensitivity.

The effect of CNTs can be appreciated by comparing the performances of Type 1 sensors in artificial and fresh sweats against their corresponding performances in buffer solution. In artificial sweat, the sensitivity decreased 71%, the LOD increased 31% and the RT decreased 44% when compared against the corresponding values obtained in buffer solution. In fresh sweat, the sensitivity decreased 85%, the LOD increased 430% and the RT decreased 33% when compared against the corresponding values obtained in buffer solution. Clearly, the more complex the medium composition the lower the sensitivity, the higher the LOD and the lower the RT. CNTs paper is an excellent substrate to immobilize GOx. However, it can also bind many other complex compounds present in sweat. Those, compounds can be responsible for hinder the access of glucose to GOx and the release of the glucono-lactone product. Which in turns can be responsible for the decrease in sensitivity and the increase of the LOD. The decrease of the RT may be a consequence of the higher concentration of electrolytes in artificial and fresh sweats when compared against buffer solution.

4. Conclusions

Glucose sensors have been fabricated to measure glucose levels in buffer solution, artificial sweat, fresh sweat and the exuded sweat of a volunteer during an exercise session. MNPs and CNPs where added to the CNTs substrate of the WE where the oxidation of glucose occurs. MNPs accelerated the RT at the expense of increasing the LOD without clear changes in the sensitivity. CNPs greatly accelerated the RT and lowered the LOD at the expense of a great diminution of the sensitivity. The phenomena were explained mechanistically. The presence of MNPs and CNPs are proposed to greatly increase the concentration of free oxygen and electrons in the CNTs substrate and induce direct effects in the activity of GOx. No previous references of using MNPs and CNPs for the detection of glucose in sweat were found. Therefore this work constitutes the first example of the application of MNPs and CNPs in epidermal bioelectronic systems for the detection of glucose in sweat.

Conflicts of interest

There are no conflicts to declare.

Acknowledgements

The authors thank the Universidad Nacional del Litoral (UNL), Consejo Nacional de Investigaciones Científicas y Técnicas (CONICET) and the Fondo para la Investigación Científica y Tecnológica (FONCYT) for the financial support. Grants: PICT 2015 1785 and PIP 1118.

References

[1] AD Association (2019) Classification and diagnosis of diabetes: Standards of medical care in diabetesd 2019. *Diabetes Care*. 42 S13–S28.

[2] C Hu, W Jia (2019) Therapeutic medications against diabetes: What we have and what we expect. *Adv. Drug Deliv. Rev*. 139 3–15.

[3] R Khursheed, SK Singh, S Wadhwa, B Kapoor, M Gulati, R Kumar, AK Ramanunny, A Awasthi, K Dua (2019) Treatment strategies against diabetes: Success so far and challenges ahead. *Eur. J. Pharmacol*. 862 172625.

[4] Z Punthakee, R Goldenberg, P Katz (2018) Definition, Classification and Diagnosis of Diabetes, Prediabetes and Metabolic Syndrome. *Can. J. Diabetes*. 42 S10–S15.

[5] Y Zhang, J Yu, AR Kahkoska, J Wang, JB Buse, Z Gu (2019) Advances in transdermal insulin delivery. *Adv. Drug Deliv. Rev*. 139 51–70.

[6] IDF (n.d.) Federación Internacional de Diabetes - Tipos de diabetes. Que Es La Diabetes.

[7] TJDRFCS Group (2008) Continuous Glucose Monitoring and Intensive Treatment of Type 1 Diabetes. *N. Engl. J Med*. 359.

[8] J Wang (2008) Electrochemical Glucose Biosensors. 814–825.

[9] B Buckingham (2008) Clinical overview of continuous glucose monitoring. *J. Diabetes Sci. Technol*. 2 300–306.

[10] RP David Olczuk (2018) A history of continuous glucose monitors (CGMs) in self-monitoring of diabetes mellitus _ Elsevier Enhanced Reader.pdf. *Diabetes Metab. Syndr. Clin. Res. Rev*. 12 181–187.

[11] JD Newman, APF Turner (2005) Home blood glucose biosensors: A commercial perspective. *Biosens. Bioelectron*. 20 2435–2453.

[12] SF Clarke, JR Foster (2012) A history of blood glucose meters and their role in self-monitoring of diabetes mellitus. *Br. J. Biomed. Sci*. 69 83–93.

[13] CE Ferrante do Amaral, B Wolf (2008) Current development in non-invasive glucose monitoring. *Med. Eng. Phys*. 30 541–549.

[14] MX Chu, K Miyajima, D Takahashi, T Arakawa, K Sano, SI Sawada, H Kudo, Y Iwasaki, K Akiyoshi, M Mochizuki, K Mitsubayashi (2011) Soft contact lens biosensor for in situ monitoring of tear glucose as non-invasive blood sugar assessment. *Talanta*. 83 960–965.

[15] J Wang, L Xu, Y Lu, K Sheng, W Liu, C Chen, Y Li, B Dong, H Song (2016) Engineered IrO2@NiO core∑shell nanowires for sensitive nonenzymatic detection of trace glucose in saliva. *Anal. Chem*. 88 12346–12353.

[16] H Lee, YJ Hong, S Baik, T Hyeon, D Kim (2018) Enzyme-Based Glucose Sensor : From Invasive to Wearable Device. 1701150 1–14.

[17] G Cappon, M Vettoretti, G Sparacino, A Facchinetti (2019) Continuous Glucose Monitoring Sensors for Diabetes Management: A Review of Technologies and Applications. *Diabetes Metab. J*. 43 383.

[18] DB Keenan, JJ Mastrototaro, G Voskanyan, GM Steil (2009) Delays in minimally invasive continuous glucose monitoring devices: A review of current technology. *J. Diabetes Sci. Technol*. 3 1207–1214.

[19] A Abellán-Llobregat, I Jeerapan, A Bandodkar, L Vidal, A Canals, J Wang, E Morallón (2017) A stretchable and screen-printed electrochemical sensor for glucose determination in human perspiration. *Biosens. Bioelectron*. 91 885–891.

[20] D Bruen, C Delaney, L Florea, D Diamond (2017) Glucose sensing for diabetes monitoring: Recent developments. *Sensors* 17 1–21.

[21] LB Baker (2019) Physiology of sweat gland function: The roles of sweating and sweat composition in human health. *Temperature* 6 211–259.

[22] M Bariya, HYY Nyein, A Javey (2018) Wearable sweat sensors. *Nat. Electron*. 1 160–171.

[23] Y Yang, W Gao (2019) Wearable and flexible electronics for continuous molecular monitoring. *Chem. Soc. Rev*. 48 1465–1491.

[24] S Robinson, H.; Robinson (1954) Chemical composition of Sweat. 11 202–220.

[25] J Choi, R Ghaffari, LB Baker, JA Rogers (2018) Skin-interfaced systems for sweat collection and analytics. *Sci. Adv*. 4 1–10.

[26] LC Alarcón-Segovia, I Rintoul (2020) Biocompatible polymers for skin-integrated bioelectronics: A Mini-Review. *Curr. Trends Polym. Sci*. 20 53–58.

[27] SY Oh, SY Hong, YR Jeong, J Yun, H Park, SW Jin, G Lee, JH Oh, H Lee, SS Lee, JS Ha (2018) Skin-Attachable, Stretchable Electrochemical Sweat Sensor for Glucose and pH Detection. *ACS Appl. Mater. Interfaces*. 10 13729–13740.

[28] Y Zhao, Q Zhai, D Dong, T An, S Gong, Q Shi, W Cheng (2019) Highly Stretchable and Strain-

Insensitive Fiber-Based Wearable Electrochemical Biosensor to Monitor Glucose in the Sweat. *Anal. Chem*. 91 6569–6576.

[29] E V. Karpova, E V. Shcherbacheva, AA Galushin, D V. Vokhmyanina, EE Karyakina, AA Karyakin (2019) Noninvasive diabetes monitoring through continuous analysis of sweat using flow-through glucose biosensor. *Anal. Chem*. 91 3778–3783.

[30] PT Toi, TQ Trung, TML Dang, CW Bae, NE Lee (2019) Highly Electrocatalytic, Durable, and Stretchable Nanohybrid Fiber for On-Body Sweat Glucose Detection. *ACS Appl. Mater. Interfaces*. 11 10707–10717.

[31] AJ Bandodkar, VWS Hung, W Jia, G Valdés-Ramírez, JR Windmiller, AG Martinez, J Ramírez, G Chan, K Kerman, J Wang (2013) Tattoo-based potentiometric ion-selective sensors for epidermal pH monitoring. *Analyst*. 138 123–128.

[32] C Shan, H Yang, D Han, Q Zhang, A Ivaska, L Niu (2010) Electrochemical determination of NADH and ethanol based on ionic liquid-functionalized graphene. *Biosens. Bioelectron*. 25 1504–1508.

[33] X Zeng, Y Zhang, X Du, Y Li, W Tang (2018) A highly sensitive glucose sensor based on a gold nanoparticles/polyaniline/multi-walled carbon nanotubes composite modified glassy carbon electrode. *New J. Chem*. 42 11944–11953.

[34] FN Comba, MD Rubianes, L Cabrera, S Gutiérrez, P Herrasti, GA Rivas (2010) Highly Sensitive and selective glucose biosensing at carbon paste electrodes modified with electrogenerated magnetite nanoparticles and glucose oxidase. *Electroanalysis*. 22 1566–1572.

[35] M Arana, CS Tettamanti, PG Bercoff, MC Rodriguez (2014) Magnetite NPs@C with highly-efficient peroxidase-like catalytic activity as an improved biosensing strategy for selective glucose detection. *Electroanalysis*. 26 1721–1728.

[36] I Rintoul, C Wandrey (2009) Magnetic field effects on the copolymerization of water-soluble and ionic monomers. *J. Polym. Sci. Part A: Polym. Chem.* 47 (2), 373-383

[37] I Rintoul, C Wandrey (2008) Radical Homo-and Copolymerization of Acrylamide and Ionic Monomers in Weak Magnetic Field. *Macromol. Symp*. 261 (1), 121-129

[38] I Rintoul (2017) Kinetic control of aqueous polymerization using radicals generated in different spin states. *Processes* 5 (2), 15

[39] AJ Bandodkar, W Jia, C Yard, X Wang, J Ramirez, J Wang (2015) Tattoo-Based Noninvasive Glucose Monitoring: A Proof-of-Concept Study.

[40] AJ Bandodkar, P Gutruf, J Choi, KH Lee, Y Sekine, JT Reeder, WJ Jeang, AJ Aranyosi, SP Lee, JB Model, R Ghaffari, CJ Su, JP Leshock, T Ray, A Verrillo, K Thomas, V Krishnamurthi, S Han, J

Kim, S Krishnan, T Hang, JA Rogers (2019) Battery-free, skin-interfaced microfluidic/electronic systems for simultaneous electrochemical, colorimetric, and volumetric analysis of sweat. *Sci. Adv*. 5 1–16.

[41] W Gao, S Emaminejad, HYY Nyein, S Challa, K Chen, A Peck, HM Fahad, H Ota, H Shiraki, D Kiriya, DH Lien, GA Brooks, RW Davis, A Javey (2016) Fully integrated wearable sensor arrays for multiplexed in situ perspiration analysis. *Nature*. 529 509–514.

[42] H Lee, C Song, YS Hong, MS Kim, HR Cho, T Kang, K Shin, SH Choi, T Hyeon, DH Kim (2017) Wearable/disposable sweat-based glucose monitoring device with multistage transdermal drug delivery module. *Sci. Adv*. 3 1–9.

[43] HBH and WRH Niina J. Ronkainen (2008) Electrochemical biosensors. *Chem. Soc. Rev*. 1747–1763.

[44] LCA Segovia, JID Agudelo, RJ Glisoni, C Acha, MM De Zan, I Rintoul. A multiparametric model for the industrialization of co-precipitation synthesis of nano-commodities. Nanotechnology. 2020, 31 (18), 185604.

[45] X Zeng, Y Zhang, X Du, Y Li, W Tang (2018) A highly sensitive glucose sensor based on a gold nanoparticles/polyaniline/multi-walled carbon nanotubes composite modified glassy carbon electrode. *New J. Chem*. 42 11944–11953.

[46] J Kimling, M Maier, B Okenve, V Kotaidis, H Ballot, A Plech (2006) Turkevich method for gold nanoparticle synthesis revisited. *J. Phys. Chem. B*. 110 15700–15707.

[47] CJ Yuan, CL Hsu, SC Wang, KS Chang (2005) Eliminating the Interference of Ascorbic Acid and Uric Acid to the Amperometric Glucose Biosensor by Cation Exchangers Membrane and Size Exclusion Membrane. *Electroanalysis* 17(24) 2239 – 2245.

[48] SM Shirreffs, RJ Maughan (1997) Whole body sweat collection in humans: an improved method with preliminary data on electrolyte content. *J. Appl. Physiol.* 82(1) 336-341.

[49] DP Kozlenko, LS Dubrovinsky, SE Kichanov, E V. Lukin, V Cerantola, AI Chumakov, BN Savenko (2019) Magnetic and electronic properties of magnetite across the high pressure anomaly. *Sci. Rep*. 9 1–9.

[50] MC Mascolo, Y Pei, TA Ring (2013) Room Temperature Co-Precipitation Synthesis of Magnetite Nanoparticles in a Large ph Window with Different Bases. *Materials* (Basel). 6 5549–5567.

[51] S Krishnamurthy, A Esterle, NC Sharma, SV Sahi (2014) Yucca-derived synthesis of gold nanomaterial and their catalytic potential. *Nanoscale Res. Lett.* 9 627

[52] X Huang, PK Jain, IH El-Sayed, MA El-Sayed (2007) Gold nanoparticles: Interesting optical properties and recent applications in cancer diagnostics and therapy. *Nanomedicine*. 2 681–693.

[53] S Jadoon, S Karim, MR Akram, AK Khan, MA Zia, AR Siddiqi, G Murtaza (2015) Recent Developments in Sweat Analysis and Its Applications. *Int. J. Anal. Chem.* 2015 164974.

[54] SC Pang , SF Chin , MA Anderson (2007) Redox equilibria of iron oxides in aqueous-based magnetite dispersions: Effect of pH and redox potential *J. Colloid Interface Sci.* 311 94–101.

[55] M Abbasi, R Amiri, AK Bordbar, E Ranjbakhsh, AR Khosropour. (2016). Improvement of the stability and activity of immobilized glucose oxidase on modified iron oxide magnetic nanoparticles. *Appl. Surf. Sci.* 364 752–757.

[56] N Sanaeifar, M Rabiee, M. Abdolrahim, M. Tahriri, D. Vashaee, L Tayebi. (2017). A novel electrochemical biosensor based on Fe3O4 nanoparticles-polyvinyl alcohol composite for sensitive detection of glucose. *Anal. Biochem.* 519.